ISSN 1070-3284, Russian Journal of Coordination Chemistry, 2020, Vol. 46, No. 2, pp. 137–144. © Pleiades Publishing, Ltd., 2020.

Synthesis, Crystallographic Structure, Hirshfeld Surface Analysis, and DFT Calculations of Two Salen-Type Hetero-Halogenated Schiff Base Mn(IV)/(III) Complexes

Q. Wu[a, b, *], J. D. Li[a], F. X. Liu[a], J. C. Xiao[a], Y. F. Tang[a], and Q. L. Zi[a]

[a] *Department of Chemical Science and Technology, Kunming University, Yunnan, Kunming, 65200 P.R. China*

[b] *Yunnan Engineering Technology Research Center for Plastic Films, Kunming, 65200 P.R. China*

**e-mail: wuqiongkm@163.com*

Received April 30, 2019; revised July 10, 2019; accepted August 14, 2019

Abstract—Two new supramolecular compounds $[Mn^{IV}(\mu\text{-}3\text{-}Br\text{-}5\text{-}Cl\text{-}Salpn)(\mu\text{-}O)]_2 \cdot 2[DMF]$ (**I**) and $[Mn^{III}(3\text{-}Br\text{-}5Cl\text{-}Salmen)(3\text{-}bromo\text{-}5\text{-}chlorosalicylaldehyde)]_2$ (**II**) (3-Br-5Cl-Salpn = *N,N'*-bis(3-bromo-5-chlorosalicylidene)-1,3-diamine and 3-Br-5Cl-Salmen = *N,N'*-bis(3-bromo-5-chlorosalicylidene)-1,2-diamine) have been synthesized via conventional solution method and characterized by single crystal (CIF files CCDC nos. 1855961 (**I**), 1900154 (**II**) and powder X-ray diffraction, IR spectroscopy and elemental analysis. The unconventional C–H···X (X = Cl and Br) supramolecular interaction within the compounds were qualitatively and quantitatively studied by Hirshfeld surface analysis. Additionally, in order to gain a deep insight into the electronic features of **I**, density functional theory was used for the calculations of the HOMO and LUMO energies and molecular electrostatic potential surface.

Keywords: halogenated Schiff-base, crystal structure, weak molecular interactions, Hirshfeld surface analysis, density functional theory calculations

DOI: 10.1134/S1070328420020086

INTRODUCTION

Supramolecular chemistry is a multidisciplinary research domain that ranges from pharmaceutics to materials science [1, 2]. It is now well known that, although the magnitude is very small, weak interactions are significant influence in the structural solid geometry and even physicochemical properties, such as activities of pharmaceutical ingredients (APIs), magnetic behavior, et al., therefore, in the past decade, great efforts have been devoted to the exploration regulating effects of physicochemical properties of different weak interactions [3, 4].

In recent years, halogen atoms have been recognized as an important factor in mediation of the supramolecular networks of crystalline materials. However, compared with the classical hydrogen bond interactions, the contact form by halogen atoms are much weaker, therefore, it is difficult to carry out qualitative and quantitative research, especially for the N- and O-rich ligands involved supramolecular complex [5, 6], hence, related work is still at a very early stage.

Therefore establishing a series of halogenated ligands constructed complexes with similar structure and composition is a fundamental way for detailed exploration of the halogen atom conducted intermolecular interactions [7, 8]. In this aspect, tetradentate Schiff base (Salen) complex is an ideal candidate, not only because their diverse structures and tunable constitution [9, 10], but also because salen-type compound is a well researched subject, subtle difference between analogs can be easily detected and more deeply studied [11, 12].

Based on the aforementioned considerations, recently, we have initiated exploitation of the relationship between the composition of Salen-type halogenated Schiff-base ligands and their special supramolecular interactions. Herein, we specifically introduced hetero-halogenated Salen-type Schiff-base ligands: *N,N'*-bis(3-bromo-5-chlorosalicylidene)-1,3-diamine (3-Br-5Cl-Salpn) and *N,N'*-bis(3-bromo-5-chlorosalicylidene)-1,2-diamine (3-Br-5Cl-Salmen) and manganate as starting materials, and isolated two new manganese complexes $[Mn^{IV}(\mu\text{-}3\text{-}Br\text{-}5\text{-}Cl\text{-}Salpn)(\mu\text{-}O)]_2 \cdot 2[DMF]$ (**I**) and $[Mn^{III}(3\text{-}Br\text{-}5Cl\text{-}Salmen)(3\text{-}bromo\text{-}5\text{-}chlorosalicylaldehyde)]_2$ (**II**). Theoretical analysis result reveal that, although the interactions formed by halogen atom are weak, halogen atoms play a key role in stabling the solid structure of title compounds.

EXPERIMENTAL

Materials and measurements. All chemicals were also commercially available and used without further purification. Elemental analyses (C, H, and N) were carried out on a Perkin-Elmer 240C instrument. The infrared (IR) spectrum was recorded from 400 to 4000 cm^{-1} on an Alpha Centaurt FT (Fourier transform) IR spectrophotometer using KBr pellets. Powder X-ray diffraction (PXRD) patterns were recorded with a Bruker D8 ADVANCE X-ray diffractometer at the room temperature.

Synthesis of halogenated Schiff base ligand. The ligands 3-Br-5Cl-Salpn and 3-Br-5Cl-Salmen were prepared by mixing 3-bromo-5-chlorosalicylaldehyde (0.047 g, 0.2 mmol) and 1,3-diaminopropane or 1,2-diaminopropane for 3-Br-5Cl-Salpn or 3-Br-5Cl-Salmen, respectively (0.0085 mL, 0.1 mmol) in methanol (30 mL). The obtained solution was stirred and refluxed at 80°C for 3 h. Then, the solvent was removed by rotary evaporator to give yellow powder product (Scheme 1).

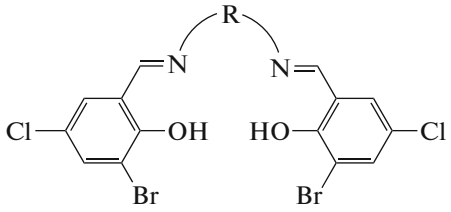

R = 1,3-diaminopropane for 3-Br-5Cl-Salpn

R = 1,2-diaminopropane for 3-Br-5Cl-Salmer

Scheme 1.

Synthesis of [Mn^{IV}(μ-3-Br-5-Cl-Salpn)(μ-O)]$_2$ · 2DMF (I). $Mn(AC)_2 \cdot 4H_2O$ (0.03675 g, 0.15 mmol) was added in a mixture solution of methanol (20 mL) and DMF (10 mL) of 3-Br-5Cl-Salpn (0.0310 g, 0.1 mmol). The black solution was stirred for 2 h. The black filtrate was sealed in a beaker and kept undisturbed at room temperature. The black block crystals of title compound were afforded after one week. The crystals were filtrated, washed with methanol, and dried in air (the yield **I** was 32%).

For $C_{40}H_{38}N_6O_8Cl_4Br_4Mn_2$ (**I**)

Anal. calcd., %	C, 36.89	H, 2.94	N, 6.45
Found, %	C, 37.53	H, 3.14	N, 6.73

IR (KBr; ν, cm^{-1}): 2930 ν(ArC–H), 2816 ν(MeC–H), 1584 ν(C=N), 1421 ν(CH_2), 1125 ν(C–O), 756 ν(C–Cl), 598 ν(C–Br).

Synthesis of [Mn^{III}(3-Br-5Cl-Salmen)(3-bromo-5-chlorosalicylaldehyde)]$_2$ (II). $Mn(AC)_2 \cdot 4H_2O$ (0.03675 g, 0.15 mmol) was added to 3-Br-5Cl-Salmen (0.0504 g, 0.1 mmol) were dissolved in methanol (30 mL), after this 3-bromo-5-chlorosalicylaldehyde (0.1 mmol, 0.0235 g) was added to the above mixture and kept stirring for 2 h, then filtered. The filtrate was sealed in a beaker and kept undisturbed at room temperature. The black block crystals of title compound were afforded after one week. The crystals were collected by suction filtration washed with methanol, and dried in air (yield of 41% based on manganese(III) acetate).

For $C_{48}H_{26}N_4O_8Cl_4Br_4Mn_2$ (**II**)

Anal. calcd., %	C, 35.45	H, 1.75	N, 4.86
Found, %	C, 34.14	H, 1.62	N, 4.42

IR (KBr; ν, cm^{-1}): 2925 ν(ArC–H), 2826 ν(MeC–H), 1626, 1590 ν(C=N), 1430 ν(CH_2), 1115 ν(C–O), 758 ν(C–Cl), 603 ν(C–Br).

X-ray crystal structure determination. The data set of reflections were collected at 296(2) K on a Xcalibur Eos automated diffractometer with MoK_α radiation (λ = 0.71073 Å) and a low-temperature device Cryostream cooler (Oxford Cryosystem). Integration of the intensities and correction for Lorentz and polarization effects were performed using the CrysAlis^{Pro} software [13, 14]. The central manganese atom was located by direct methods, and successive Fourier syntheses revealed the remaining atoms. Refinements were achieved by the full-matrix method on F^2 using the Olex2 software package [15]. In the final refinement, all the non-H atoms were anisotropically refined. All H atoms were placed in calculated positions and refined using the riding model approximation. For compound **I**, C–H bonds of methyl and methylene group were fixed at 0.98 and 0.99 Å, respectively; for compound **II**, C–H bonds of methyl group were fixed at 0.96 Å. The detailed crystal data and structure refinement for **I** and **II** were given in Table 1. Selective bond lengths and angles of **I** and **II** were listed in Table 2.

The crystal data can be obtained free of charge from Cambridge Crystallographic Data Centre (CCDC nos. 1855961 (**I**), 1900154 (**II**); www.ccdc.cam.ac.uk/data_request/cif).

RESULTS AND DISCUSSION

As shown in Fig. 1a, the basic unit of compound **I** consists of a Mn(IV) dimer structure in which two hetero-halogenated Salen-type Schiff-base ligands ride both Mn^{4+} ions via two nitrogen atoms in the stereoscopic mode, then, two μ-2 oxygen atoms further bridge the metal atoms yield a planar Mn_2O_2 center core, this kind of bridging mode is similar to that of previously reported structure [16], noteworthy that these two oxygen atoms are assigned as bridging atoms μ-2 O^{2-} rather than H_2O nor to OH^- is based on the bond valence sum (BVS) calculations and symmetry about the central core [17]. Therefore, each Mn^{4+} ions

Table 1. Crystallographic data and structure refinement for compounds **I** and **II**

Parameter	Value	
	I	**II**
Mr	1302.08	1588.71
Temperature, K	173(2)	293(2)
Wavelength, Å	0.71073	0.71073
Crystal system	Triclinic	Monoclinic
Space group	$P\bar{1}$	$P2_1/c$
a, Å	10.207(2)	13.4540(11)
b, Å	10.9368(14)	15.4193(9)
c, Å	11.9899(11)	14.479(2)
α, deg	102.911(9)	90
β, deg	95.437(13)	118.297(8)
γ, deg	116.110(17)	90
Volume, Å^3	1142.6(3)	2644.8(5)
Z	1	2
Calculated density, mg/m^3	1.892	1.995
Absorption coefficient, mm^{-1}	4.342	5.370
F(000)	642	1536
θ Range for data, deg collection, deg	3.57–25.00	3.57–25.00
Limiting indices	$-10 \le h \le 12$, $-12 \le k \le 12$, $-14 \le l \le 14$	$-15 \le h \le 15$, $-18 \le k \le 18$, $-17 \le l \le 14$
Reflections collected/unique (R_{int})	7650/4006 (0.0668)	15692/4637 (0.0885)
Completeness to θ = 25.00, %	99.7	99.6
Refinement method	Full-matrix least-squares on F^2	Full-matrix least-squares on F^2
Data/restraints/parameters	4006/0/289	4637/21/345
Goodness-of-fit on F^2	0.975	1.026
Final *R* indices ($I > 2\sigma(I)$)	$R_1 = 0.0591$, $wR_2 = 0.0758$	$R_1 = 0.0735$, $wR_2 = 0.1533$
R indices (all data)	$R_1 = 0.1008$, $wR_2 = 0.0910$	$R_1 = 0.1453$, $wR_2 = 0.1943$
Largest diff. peak and hole, e Å^{-3}	0.652 and –0.642	0.919 and –0.939

is in a distorted octahedral coordination environment [MnO_4N_2]. Specifically, the equatorial plane of Mn(IV) center is occupied by two phenol oxygen atoms (O(1) and O(2)) from two different 3-Br-5Cl-Salpn ligands and two bridging oxo atoms (O(3) and O(3)^1 (^{1} $3-x, 1-y, 1-z$)). The axial sites are defined by also two imine nitrogen atoms derived from two different Schiff bases ligands, the distance of Mn(1)–N(1) and Mn(1)–N(2) is 2.012(5) and 1.991(5) Å. The distance of Mn–O_{phenol} is 1.935(4) and 1.929(4) Å, the observed value of **I** is in accordance with previously reported di-μ-oxo-bridged Mn(IV) dimer structures [18, 19].

According to the analysis of result of PLATON software [20], phenoxy oxygen atom from DMF formed C–H···O hydrogen bonds and chlorine atom formed C–H···Cl hydrogen bonds play a key role in stabilizing the crystal structure, which result is consist with the Hirshfeld surface analysis. As illustrated in Fig. 1b, the adjacent dimers are connected by intermolecular C–H···O and C–H···Cl hydrogen bonding interactions C(7)–H(7*A*)···O(4) (D···A 3.230(8) Å, D–H···A 137°) and C(17)–H(17*B*)···Cl(1) (D···A 3.680(9) Å, D–H···A 145°) to generate one-dimensional chain structure along the crystallographic *b*-axis.

The asymmetric unit of compound **II** contains one 3-Br-5Cl-Salmen salen-type ligand, one manganese(III) ion and one 3-bromo-5-chlorosalicylaldehyde anion (Fig. 1c). The basal plane of Mn(III) cen-

Table 2. Selected bond distances (Å) and angles (deg) for the complexes **I** and **II***

Bond	*d*, Å	Bond	*d*, Å
		I	
Mn(1)–O(3)[1]	1.801(4)	Mn(1)–O(1)	1.935(4)
Mn(1)–O(3)	1.810(4)	Mn(1)–N(1)	1.991(5)
Mn(1)–O(2)	1.929(4)	Mn(1)–N(2)	2.012(5)
Cl(1)–C(3)	1.739(6)	Br(1)–C(5)	1.894(6)
Cl(2)–C(11)	1.741(6)	Br(2)–C(13)	1.896(6)
* Symmetry codes for complex **I**: [1] $-x+3, -y+1, -z+1$.			
		II	
Mn(1)–O(2)	1.864(5)	Mn(1)–N(2)	2.000(6)
Mn(1)–O(1)	1.883(5)	Mn(1)–O(3)	2.027(5)
Mn(1)–N(1)	1.973(6)		
Cl(1)–C(4)	1.711(7)	Br(1)–C(2)	1.863(7)
Cl(2)–C(13)	1.713(8)	Br(2)–C(15)	1.884(9)
Cl(3)–C(21) 1.731(10) ?	1.731(10)	Br(3)–C(19)	1.894(8)
Angle	ω, deg	Angle	ω, deg
		I	
O(3)[1]Mn(1)O(3)	80.8(2)	O(3)Mn(1)N(1)	92.1(2)
O(3)[1]Mn(1)O(2)	172.40(19)	O(2)Mn(1)N(1)	84.1(2)
O(3)Mn(1)O(2)	91.9(2)	O(1)Mn(1)N(1)	89.16(19)
O(3)[1]Mn(1)O(1)	92.28(19)	O(3)[1]Mn(1)N(2)	93.8(2)
O(3)Mn(1)O(1)	173.0(2)	O(3)Mn(1)N(2)	94.35(18)
O(2)Mn(1)O(1)	95.07(19)	O(2)Mn(1)N(2)	88.8(2)
O(3)[1]Mn(1)N(1)	94.07(19)	O(1)Mn(1)N(2)	85.29(19)
* Symmetry codes for complex (**I**): [1] $-x+3, -y+1, -z+1$.			
		II	
O(2)Mn(1)O(1)	94.1(2)	N(1)Mn(1)N(2)	82.1(3)
O(2)Mn(1)N(1)	163.7(2)	O(2)Mn(1)O(3)	100.9(2)
O(1)Mn(1)N(1)	89.7(2)	O(1)Mn(1)O(3)	96.1(2)
O(2)Mn(1)N(2)	90.5(2)	N(1)Mn(1)O(3)	94.5(2)
O(1)Mn(1)N(2)	164.7(3)	N(2)Mn(1)O(3)	97.4(3)

ter of **II** is chelated by O(1), O(2), N(1), and N(2) from 3-Br-5Cl-Salmen, the bond lengths of Mn–O(N) are in the range of 1.864(5)–2.027(5) Å, while bond angles of O(N)MnO vary from 80.8(2)° to 173.0(2)°. The dihedral angle calculated between the planes of two benzene rings for **II** is 13.807(235)°. Thus, the moiety overall exhibit *Z*-type distortion. The apical positions of **II** are occupied by one oxygen atom O(3) from 3-bromo-5-chlorosalicylaldehyde anion and one oxygen atom O(1)[1] ([1] $1-x, -1-y, 1-z$)) from phenolate group of other halve of 3-Br-5Cl-Salmen ligand, the bond length of Mn(1)–O(3) and Mn(1)–O(1)[1] is 2.028 and 2.954 Å, respectively. Further analysis shows that aldehyde oxygen atoms formed intermolecular hydrogen bonding C(10)–H(10)···O(4) (D···A 3.403(10) Å, D–H···A 156°) play an important part in linking the neighbouring molecules to form two-dimensional lay structure (Fig. 1d).

In order to check the phase purities of complexes **I** and **II**, the XRD patterns have been checked at ambient temperature. As shown in Fig. 2, for both compounds, the simulated patterns agreed well with those of the experimental patterns, indicating phase purities of the as-synthesized samples. The slight differences in reflection intensity between the simulated and experimental patterns are due to the variation in crystal orientation of the powder samples.

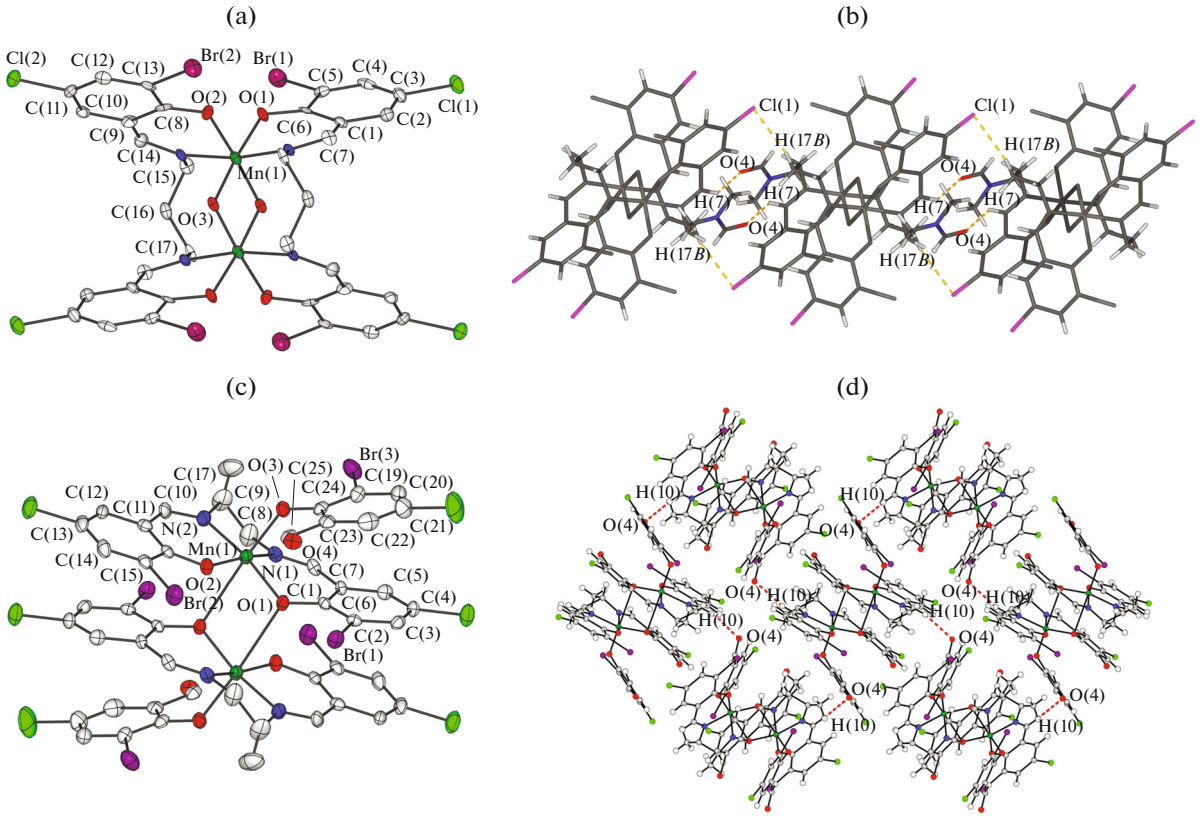

Fig. 1. Molecular structure of complex **I** (a), supramolecular interactions of complex **I** showing the intermolecular hydrogen bonding formed one-dimensional chain structure (b), ball-and-stick representation of complex **II** (c), the intermolecular hydrogen bonding formed two-dimensional layer structure of complex **II** (d).

It is noteworthy that according to the analysis of result of PLATON software [18], seemingly that except aldehyde oxygen from 3-bromo-5-chlorosalicylaldehyde formed C–H···O interactions (Table 3), there is no other intermolecular hydrogen bond exist in the crystal structure. By comparison, Hirshfeld surface analysis give us a more specific qualitative and quantitative contributions of the interactions in the crystal packing. Detailed discussion is addressed in Hirshfeld surface analysis section.

The bundle of inter-related weak molecular interactions is difficult to be unraveled by traditional methods [21]. Hirshfeld surface analysis offer us a new perspective on the issue. This analysis method can provide detailed explanation about the nearby environment of the molecules in a crystal, and the comparison between similar structures can give a more specific description of the difference [22]. Hirshfeld surface in the 2D fingerprint plots show that (Fig. 3a), for compound **I**, the Cl···H/H···Cl and Br···H/H···Br interaction covers the highest proportion (33.4%) of the total plots, whereas, the proportion C–H···C and C–H···O contacts only cover 25.5%, which is much smaller than the halogen atom involved contacts.

Hirshfeld surface in the 2D fingerprint for compound **II** is similar with that of **I** (Fig. 3b), the major intermolecular interaction is also contribute by halogen atoms, and the Cl···H/H···Cl and Br···H/H···Br interaction covers the highest proportion (42.5%) of the total plots, whereas, the C–H···C and C–H···O contacts only cover less than a half proportion of Cl···H/H···Cl and Br···H/H···Br interaction, merely comprising 19.2% of the total Hirshfeld surface. These results indicate that albeit halogen formed hydrogen bond interaction is weak, halogen atoms in **I** and **II** play the most important part in stabilizing the solid stature.

The frontier molecular orbitals (FMOs) is an important theoretical method in providing information about kinetic stability, energy levels and molecular reactivity. All of the calculations were done by Gaussian 09 software. Density functional theory (DFT) with the B3LYP functional levels for the 6-311G (d, p) basis set was used for complete calculations [23]. Figure 4a shows the distributions and energy levels of the HOMO–LUMO orbitals computed at the B3LYP level for **I**. The value of the energy separation between the HOMO and LUMO is –2.97 and –6.12 eV, respectively. The magnitude of the energy separation between the HOMO and LUMO is

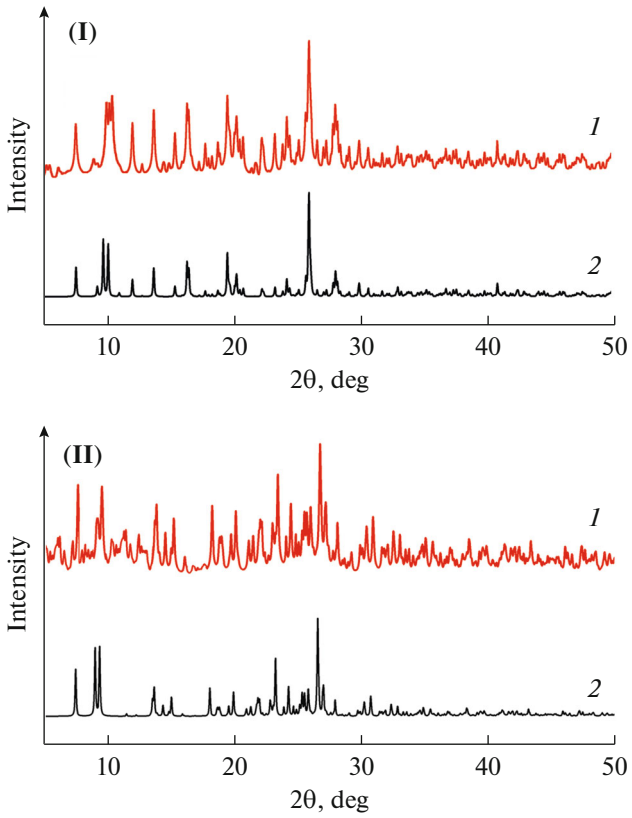

Fig. 2. Experimental (*1*) and simulated (*2*) XRPD patterns of **I** and **II** at room temperature.

3.15 eV. This relatively high value indicates the good stability of the title structure.

To further compare the weak interactions and chemical reactivity of **I**, the molecular electrostatic potential (MEP) surface map of the compounds was investigated with theoretical calculations at the B3LYP/6-311G (d,p) level. In Fig. 4b, MEP is shown. As expected, the most negative electrostatic potential corresponds to the region between the phenolic oxygen atom, also influenced by the halogen atoms. This nucleophile site (negative potential value of –26.2 kcal mol^{-1}) is distributed around the oxygen atom due to the intermolecular C–H···O and C–H···Cl interactions. The most positive region is observed in the region of the 1,3-diaminopropane group at the molecular plane (29.9 kcal mol^{-1}). This result is in accordance with the single-crystal structure analysis.

In summary, two new salen-type halogenated Schiff-base Mn(IV)/Mn(III) complexes have been synthesized by conventional method. The structures have been determined by the single crystal X-ray diffraction, IR and XRD techniques. Hirshfeld surface analysis and DFT calculations have been employed to further analyze the inter/intramolecular interactions, all the results agree well with the single-crystal structure analyses. The detailed comparison of Hirshfeld surface analysis result indicates that Cl···H/H···Cl and Br···H/H···Br interaction cover a quite high proportion in solid structures. That is to say, although the interactions formed by halogen atom are weak, halogen atoms can play an important role in directing and stabilizing the solid structures of Schiff-base complexes. As different supramolecular interaction can lead a totally different physicochemical properties, further work will continue focusing on the synthesis of halogenate ligands constructed complexes to systematically explore the regulating effect of halogen atoms.

Table 3. Geometric parameters of hydrogen bond distances (Å) and angles (deg) for the complexes **I** and **II**

D–H···A	Distance, Å		Angle DHA, deg
	H···A	D···A	
I			
C(7)–H(7*A*)···O(4)[1]	2.47	3.230(8)	137
C(15)–H(15*A*)···O(3)	2.58	3.027(8)	108
C(15)–H(15*A*)···O(1)[1]	2.56	3.041(8)	109
C(16)–H(16*A*)···O(3)	2.52	2.980(9)	108
C(16)–H(16*A*)···O(2)[1]	2.55	2.993(8)	107
C(17)–H(17*B*)···Cl(1)[2]	2.83	3.680(9)	145
C(18)–H(18*A*)···O(4)	2.37	2.786(11)	105
* Symmetry codes for complex **I**: [1] $1-x, 1-y, 1-z$, [2] $1-x, -y, 1-z$.			
II			
C(8)–H(8)···Br(1)[1]	2.81	3.676(11)	147
C(10)–H(10)···O(4)[2]	2.53	3.403(10)	156
* Symmetry codes for complex **II**: [1] $1-x, -y, -z$, [2] $-x, -1/2+y, 1/2-z$.			

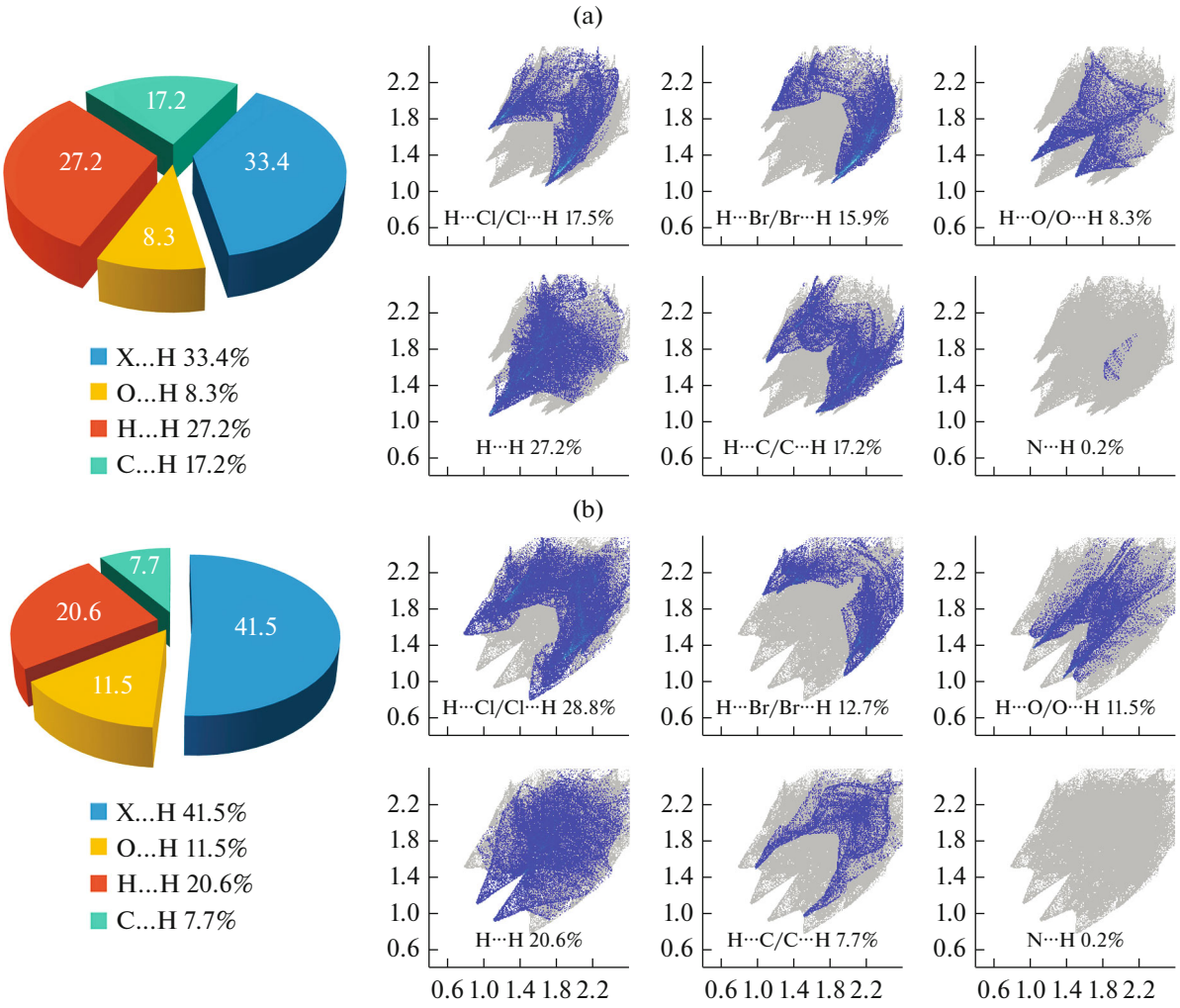

Fig. 3. Two dimensional fingerprint plots of the complex **I** (a) and **II** (b): resolved contacts showing the percentages of the weak contacts contributed to the total Hirshfeld Surface area of the title compounds (left), columns highlight the relevant surface patches associated with the specific contacts in the total Hirshfeld Surface area of the title compounds (right).

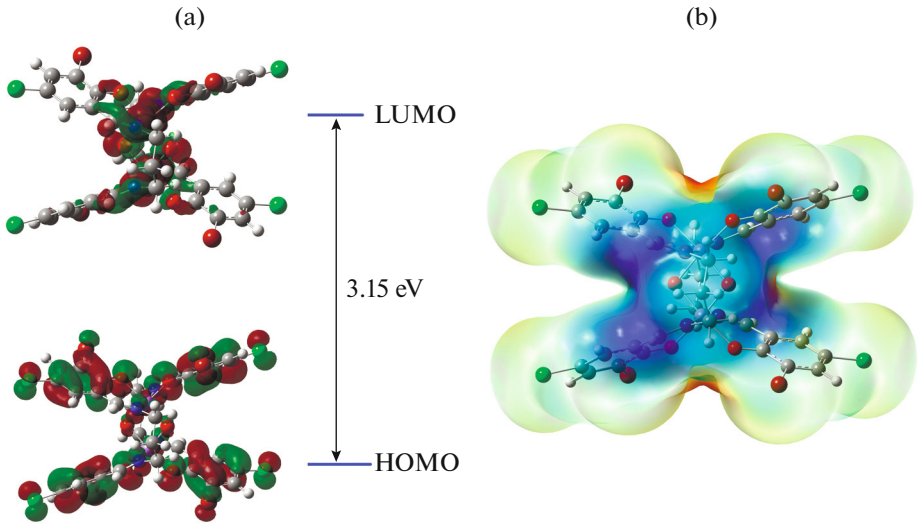

Fig. 4. Molecular orbital surfaces for the HOMO and LUMO of **I** computed at B3LYP/6-311G (d, p) level (a); the molecular electrostatic potential surface of **I** (b).

FUNDING

This work was supported by Fund for Less Developed Regions of the National Natural Science Foundation of China (no. 31760257); Joint Basic Research Program (partial) of Yunnan Local Undergraduate Universities (2017FH001-002); The the reserve academic and technical leaders of Yunnan Province (2019HB098); The Kunming University Chemistry and Chemical Engineering Students' Science and Technology Innovation Project HXHG1808.

REFERENCES

1. Huang, F. and Anslyn, E.V., *Chem. Rev.*, 2015, vol. 115, no. 15, p. 6999.
2. Slater, A.G., Perdigao, L.M., Beton, P.H., and Champness, N.R., *Accounts Chem. Res.*, 2014, vol. 47, no. 12, p. 3417.
3. Wu, Q., Tang, Y., and Zi, Q., *Polyhedron*, 2019, vol. 166, p. 123.
4. Lecren, L., Wernsdorfer, W., Li, Y.G., et al., *J. Am. Chem. Soc.*, 2007, vol. 129, no. 16, p. 50451.
5. Ma, C., Tian, G., and Zhang, R., *J. Organomet. Chem.*, 2006, vol. 691, no. 9, p. 2014.
6. d'Arová, M., Sivák, M., Kuchta, L., et al., *Dalton Trans.*, 2004, vol. 2004, no. 20, p. 3313.
7. Phonsri, W., Macedo, D.S., Vignesh, K.R., et al., *Chem. Eur. J.*, 2017, vol. 23, no. 29.
8. Armentano, D., Barquero, M.A., Rojasdotti, C., et al., *Cryst. Growth Des.*, 2017, vol. 17, no. 10.
9. Egekenze, R., Gultneh, Y., and Butcher, R., *Polyhedron*, 2018, vol. 144, p. 198.
10. Hazari, A., Gomez-Garcia, C.J., Drew, M.G.B., and Ghosh, A., *Polyhedron*, 2017, vol. 138, p. 145.
11. Shao, L., Chen, Q., and Qi, C., *Kinet. Catal.*, 2017, vol. 58, no. 6, p. 758.
12. Xue, C., Zhang, H., and Zhang, D.P.R., *J. Coord. Chem.*, 2017, vol. 43, no. 4, p. 260.
13. *CrysAlis^{Pro}, Version 1.171.35.19*, Santa Clara: Agilent Technologies Inc., 2011.
14. *CrysAlis^{PRO}, Software System, Version 1.171.39.9g*, Oxford: Agilent Technologies, 2015.
15. Dolomanov, O.V., Bourhis, L.J., Gildea, R., et al., *J. Appl. Crystallogr.*, 2010, vol. 42, no. 2, p. 339.
16. Bermejo, M.R., Castineiras, A., Garcia-Monteagudo, J.C., et al., *Dalton Trans.*, 1996, no. 14, p. 2935.
17. Brown, I.D. and Altermatt, D., *Acta Crystallogr., Sect. B: Struct. Sci.*, 1985, vol. 41, no. 4, p. 244.
18. Maneiro, M., Bermejo, M., Fondo, M., et al., *Polyhedron*, 2001, vol. 20, no. 7, p. 711.
19. Law, N.A., Kampf, J.W., and Pecoraro, V.L., *Inorg. Chim. Acta*, 2000, vol. 297, no. 1, p. 252.
20. Spek, A.L.J., *J. Appl. Crystallogr.*, 2003, vol. 36, no. 1, p. 7.
21. Spackman, M.A. and Jayatilaka, D., *CrystEngComm*, 2009, vol. 11, no. 1, p. 19.
22. McKinnon, J., Spackman, M.A., and Mitchell, A.S., *Acta. Crystallogr. Sect. B: Struct. Sci.*, 2004, vol. 60, no. 6, p. 627.
23. Andersson, M.P. and Uvdal, P., *J. Phys. Chem., A*, 2005, vol. 109, no. 12, p. 2937.